Zwitterionic Nanomicelle Self-Assembly Reconstructs Interfacial Chemistry toward Durable Zinc Anode

Yuchong Peng,[a-b] Zhaoyu Zhang,[a-b] Guoli Liao,[a-b] Wencheng Du,[a-b] Yufei Zhang,[a-b] Minghui Ye,[a-b] Zhipeng Wen,[a-b] Yongchao Tang,[a-b] Xiaoqing Liu,[a-b] and Cheng Chao Li[a-b]**

[a] Y. Peng, Z. Zhang, G. Liao, W. Du, Y. Zhang, M. Ye, Z. Wen, Y. Tang, Prof. X. Liu, and Prof. C. C. Li
School of Chemical Engineering and Light Industry, Guangdong University of Technology, Guangzhou 510006, China

[b] Y. Peng, Z. Zhang, G. Liao, W. Du, Y. Zhang, M. Ye, Z. Wen, Y. Tang, Prof. X. Liu, and Prof. C. C. Li
Guangdong Provincial Laboratory of Chemistry and Fine Chemical Engineering Jieyang Center, Jieyang 515200, China

Experimental Section

Chemicals: Zn foil (99.995%, Guangdong Canrd New Energy Technology Co., Ltd), Cu foil (99.99%, Guangdong Canrd New Energy Technology Co., Ltd), Zinc sulfate heptahydrate ($ZnSO_4 \cdot 7H_2O$, Aladdin), 3-[Dimethyl-[2-(2-methylprop-2-enoyloxy)ethyl]azaniumyl]propane-1-sulfonate (SPE, ≥98%, Macklin), Super P (Guangdong Canrd New Energy Technology Co., Ltd), Ammonium metavanadate (NH_4VO_3, ≥99.95%, Aladdin), Oxalic acid dihydrate ($C_2H_2O_4 \cdot 2H_2O$, 99.5%, Mackin). All reagents were used as received without further purification.

Electrolyte preparation: A homogeneous 0.5 mol/L (M) aqueous zinc sulfate ($ZnSO_4$) electrolyte was prepared by adding a certain amount of zinc sulfate heptahydrate ($ZnSO_4 \cdot 7H_2O$) to deionized water followed by stirring. In addition, by adding a calculated amount of SPE to the 0.5 mol/L (M) zinc sulfate electrolyte, x mol/L (M) SPE electrolytes were obtained (x = 0.01, 0.05, 0.15, 0.25, 0.4), *i.e.*, the electrolyte system consists of 0.5 mol/L zinc sulfate + x mol/L SPE.

Preparation of $NH_4V_4O_{10}$ cathode material: $NH_4V_4O_{10}$ cathode material was synthesized via a conventional hydrothermal approach.[1] Specifically, 1.17 g of NH_4VO_3 was dissolved into 35 mL deionized water at 80 °C, forming a pale yellow aqueous solution. Subsequently, 1.891 g of $H_2C_2O_4 \cdot 2H_2O$ was added to the solution, and the resultant mixture was subjected to continuous magnetic stirring until it turned into a dark green homogeneous system. The obtained solution was subsequently transferred to a 50 mL Teflon-lined autoclave, which was sealed tightly and maintained in an oven at 140 °C for 48 h. After cooling naturally to room temperature, the precipitate was recovered, rinsed repeatedly with deionized water, and finally dried at 80 °C to acquire the target product. The $NH_4V_4O_{10}$ electrode was constructed by blending $NH_4V_4O_{10}$, Super P, and polyvinylidene fluoride (PVDF) with a weight ratio of 7:2:1. The mixture was dispersed in N-methyl-2-pyrrolidone (NMP) and stirred magnetically for 24 h to yield a homogeneous slurry. This slurry was then spread onto stainless steel foil (300 mesh, 99.5% purity) and dried in a vacuum drying oven at 80 °C for over 12 h, resulting in $NH_4V_4O_{10}$ cathodes with a mass loading of around 2 mg cm^{-2}.

Materials characterization: ^{1}H-NMR spectra of the samples were performed on a JNM-ECZ500R/S1 500 MHz superconducting Fourier using deuterium oxide (D_2O) as solvent. Fourier transform infrared

spectroscopy (FTIR) measurements were performed using an iS50R (THEMOR-FILSHER, USA). All FTIR experiments were conducted in attenuated total reflection (ATR) mode. Raman spectra were recorded using HORIBA, LabRAM HR800 at room temperature with laser excitation at 532 nm. The Zeta values were measured by the Nano Particle Size and Zeta Potential Analyzer (Malvern Zetasizer Nano ZS). The crystalline structure of the samples was characterized by X-ray powder diffraction (XRD, Rigaku SmartLab, Cu-Kα radiation, λ = 1.54 Å) at a range of 2θ = 5~80°. Confocal laser scanning microscope (CLSM) images were obtained by Olympus, OLS4100. X-ray photoelectron spectroscopy (XPS) was used to determine the surface chemical composition of the samples (Escalab 250Xi, Thermo Fisher). The scanning electron microscope (SEM, Hitachi S-3400 N) was used to observe the morphology and elemental composition of the samples.

Simulation methods: MD simulations were performed in GROMACS using the General Amber Force Field (GAFF). Topology files and bonded and Lennard-Jones parameters were generated by using the Autoff, while the RESP atomic charges from Multiwfn3.8 program were used.[2] The cutoff for the Lennard-Jones potential was set to 12 Å. The long-range Coulombic interactions were counted by a particle–particle particle-mesh. The initial periodic systems were set up using PACKMOL.[3] The ratio of each type of molecule was based on the molar ratio of each molecule of the system. All ions and molecules were inserted in an initial cube box with 10 nm sides. In the equilibrium stage of the system, the energy of the simulated system was minimized by the conjugate gradient method first, then the equilibrium simulation was carried out under NPT ensemble for 10 ns, with the temperature at 300 K and the pressure at 1 atm. Finally, the simulation was continued for 20 ns with NVT ensemble and data were collected. Only the final 5-ns trajectory was sampled for the analysis of radial distribution function and solvent-solute interaction environments.

Density functional theory (DFT) calculations were performed with the Gaussian 16 software at the B3LYP/6-311G* level to optimize the molecular geometries of these structures. Subsequently, binding energies were computed for these optimized structures at the B3LYP/6-311+G(d,p) level.

All zinc crystal surface adsorption models were constructed using Matter Craft software. (Matter Craft Version 4.4.4; Shenzhen Eacomp Technology Co., Ltd.: Shenzhen, China, 2020.) First-principles calculations were performed within the framework of density functional theory via the plane-wave pseudopotential method implemented in the Hylanemos package[4] embedded in Matter Craft. The

Perdew−Burke−Ernzerhof (PBE) exchange-correlation functional within the generalized gradient approximation (GGA) was employed. The kinetic energy cutoff for the plane-wave basis set was set to 450 eV. Brillouin zone integrations were performed using a Monkhorst−Pack k-point mesh of 2 × 2 × 1. Grimme's D3 dispersion correction was considered to include the van der Waals interactions. To avoid artificial interaction between neighboring images, a vacuum spacing of more than 25 Å was introduced in the surface calculations.

The adsorption energy (ΔE) was determined according to the formula:

$$\Delta E = E_{AB} - (E_A + E_B)$$

where E_{AB} represents the total energy of the combined system, while E_A and E_B correspond to the total energies of the isolated constituent components, respectively.

Electrochemical testing: Zn||Zn symmetric battery, Zn||Cu asymmetric battery and Zn||NVO ($NH_4V_4O_{10}$) full battery were manufactured based on the CR2032 coin cell configuration. The electrolyte volume of each battery is 160 μL. When assemble the battery, the electrodes are separated by glass fiber separators (GF/D, Whatman) at room temperature. In this study, the zinc foil with a diameter of 12 mm and the separators with diameter of 16 mm were used. In the three-electrode system, Ag/AgCl, Pt plate and Zn foil are used as reference, counter and working electrodes, respectively. These electrodes were used to record cyclic voltammetry (CV), linear scanning voltammetry (LSV), and Tafel curves in 0.5 M ZSO and 0.15 M SPE on a Gamry electrochemical workstation at a scan rate of 1 mV s^{-1}. LSV tests were performed within a voltage range of −0.9 to −1.6 V.

The relationship between nucleation particle size and over-potential is represented by the following equation:[5, 6]

$$\gamma_{crit} = \frac{2\gamma V_m}{F|\eta|}$$

The classical nucleation equation includes the critical radius of a spherical nuclei (γ_{crit}), the surface energy of the Zn-electrolyte interface (γ), the molar volume of Zn (V_m), the Faraday constant (F), and the nucleation over-potential (η), respectively.

Electrochemical impedance spectroscopy (EIS) measurements were performed on a Gamry electrochemical workstation in the frequency range of 0.01 Hz to 100 kHz.

Zn||NVO full cells were assembled into 2032-type coin cells by sandwiching a Zn anode, a glass fiber filter (Whatman, GF/D) and an NVO cathode using electrolyte (160 µL) in 0.5 M ZSO or 0.15 M SPE. Galvanostatic charge/discharge tests were performed on a Neware battery test system (model CT-4008-10V 50mA-164, from Shenzhen) within an electrochemical window of 0.4 to 1.4 V.

Table S1 Ionic conductivity and viscosity of 0.5 M ZSO solutions with varying concentrations of SPE

The concentration of SPE （mol/L）	Ion conductivity (mS/cm)	Viscosity (mPa·S)
0	14.53	4.19
0.01	15.72	4.27
0.05	16.63	4.36
0.15	17.03	4.43
0.25	17.24	4.58
0.4	16.32	4.77

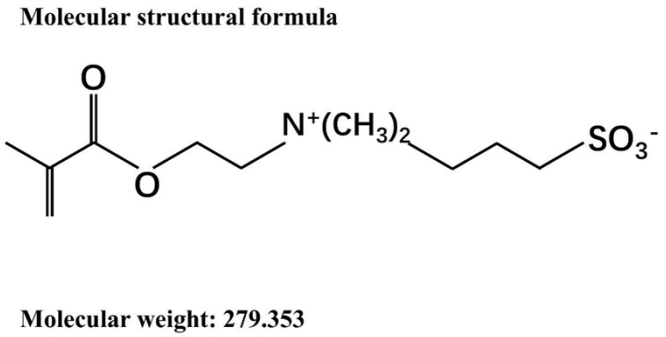

Figure S1. The molecular formula and molecular weight of SPE.

Figure S2. Optical photographs of ZSO electrolytes containing various molar mass of SPE additives (0 M, 0.01 M, 0.05 M, 0.15 M, 0.25 M, 0.4 M).

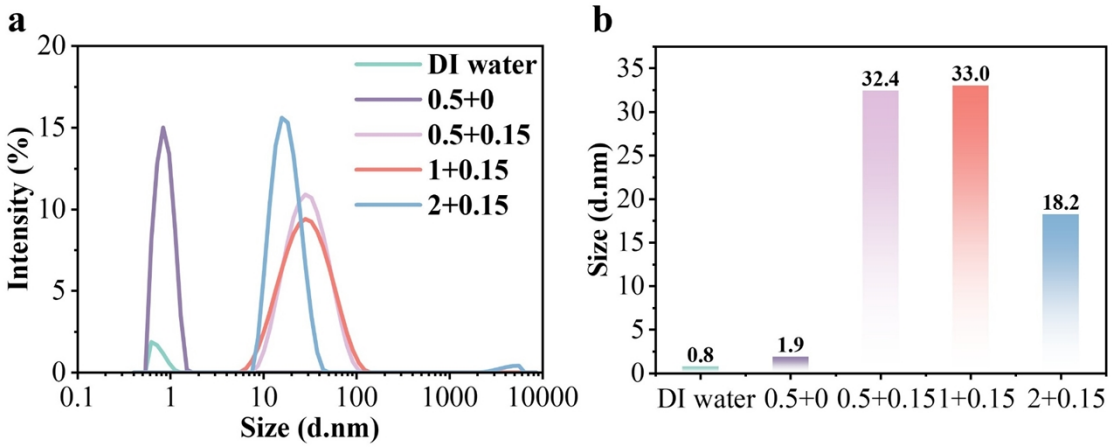

Figure S3. a) DLS analysis spectra of different electrolytes. b) Average particle size of nanoclusters in different electrolytes.

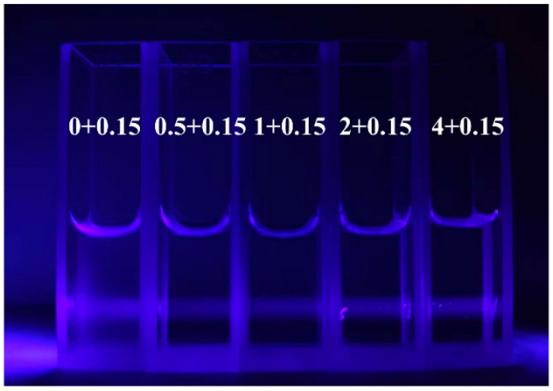

Figure S4. Tyndall Effect of 0.15 M SPE in $ZnSO_4$ Solutions with different concentrations.

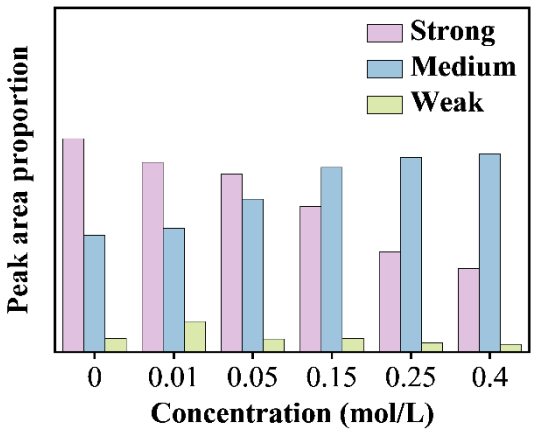

Figure S5. The proportion of different types of hydrogen bonds in SPE electrolytes of different concentrations.

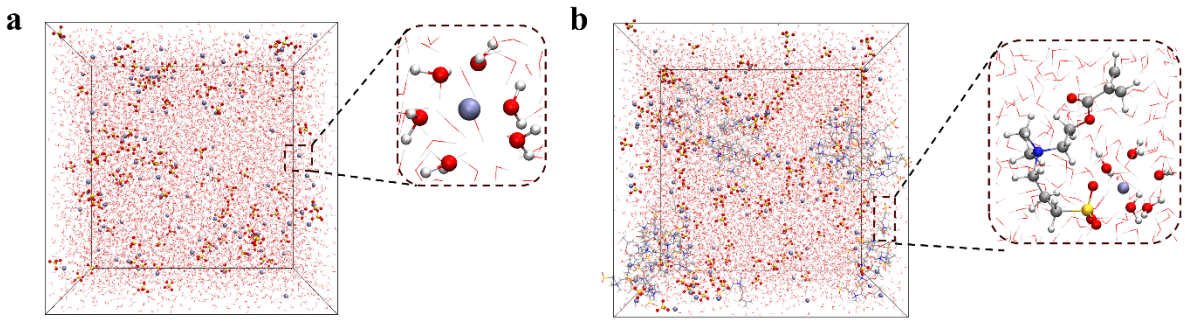

Figure S6. Three-dimensional snapshots of Zn^{2+} in a) 0.5 M ZSO and b) 0.15 M SPE electrolytes obtained via molecular dynamics (MD) simulations, along with partially enlarged snapshots illustrating the solvation structure of Zn^{2+}.

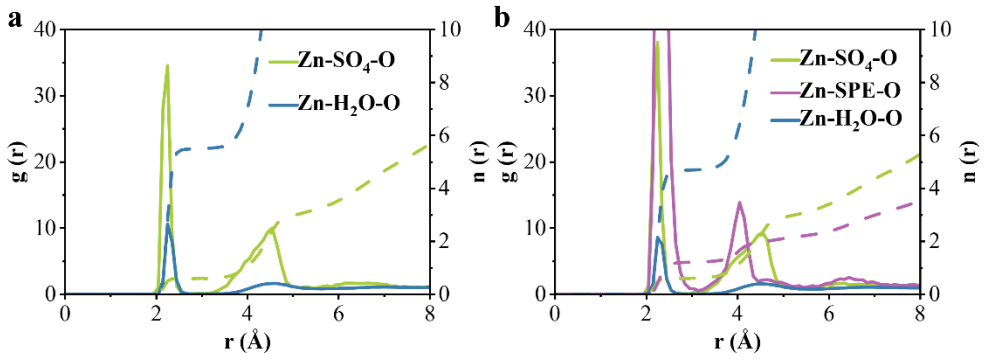

Figure S7. Radial distribution functions of Zn^{2+}-O (water), Zn^{2+}-O (SO_4^{2-}), Zn^{2+}-O (SPE) and the coordination number in a) 0.5 M ZSO b) 0.15 M SPE electrolytes.

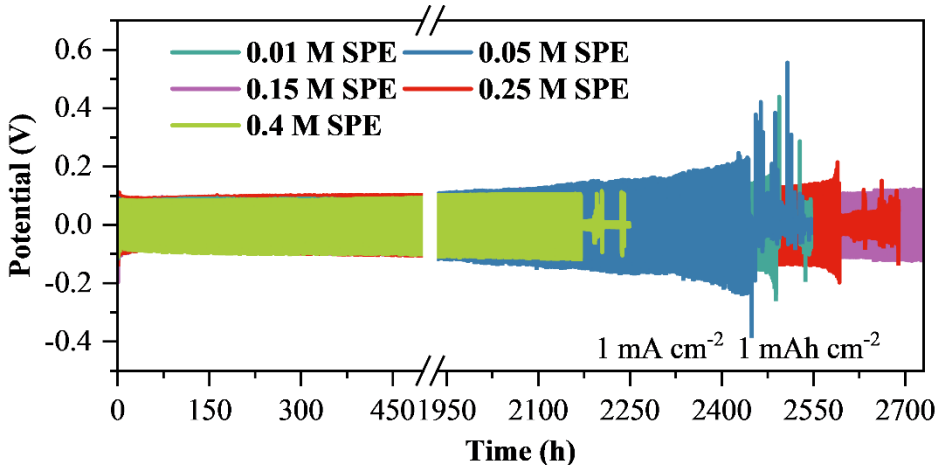

Figure S8. Cycle performance of Zn symmetric cells in electrolytes in 0.5 M ZSO electrolyte with different concentrations of SPE additive at 1 mA cm^{-2}, 1 mAh cm^{-2}.

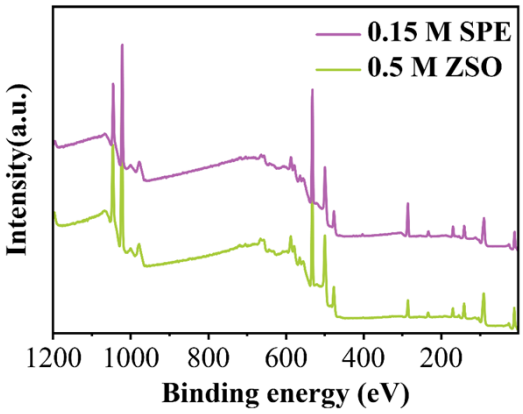

Figure S9. The full XPS spectra of deposited Zn anode in 0.5 M ZSO electrolyte, and deposited Zn anode in 0.15 M SPE electrolyte.

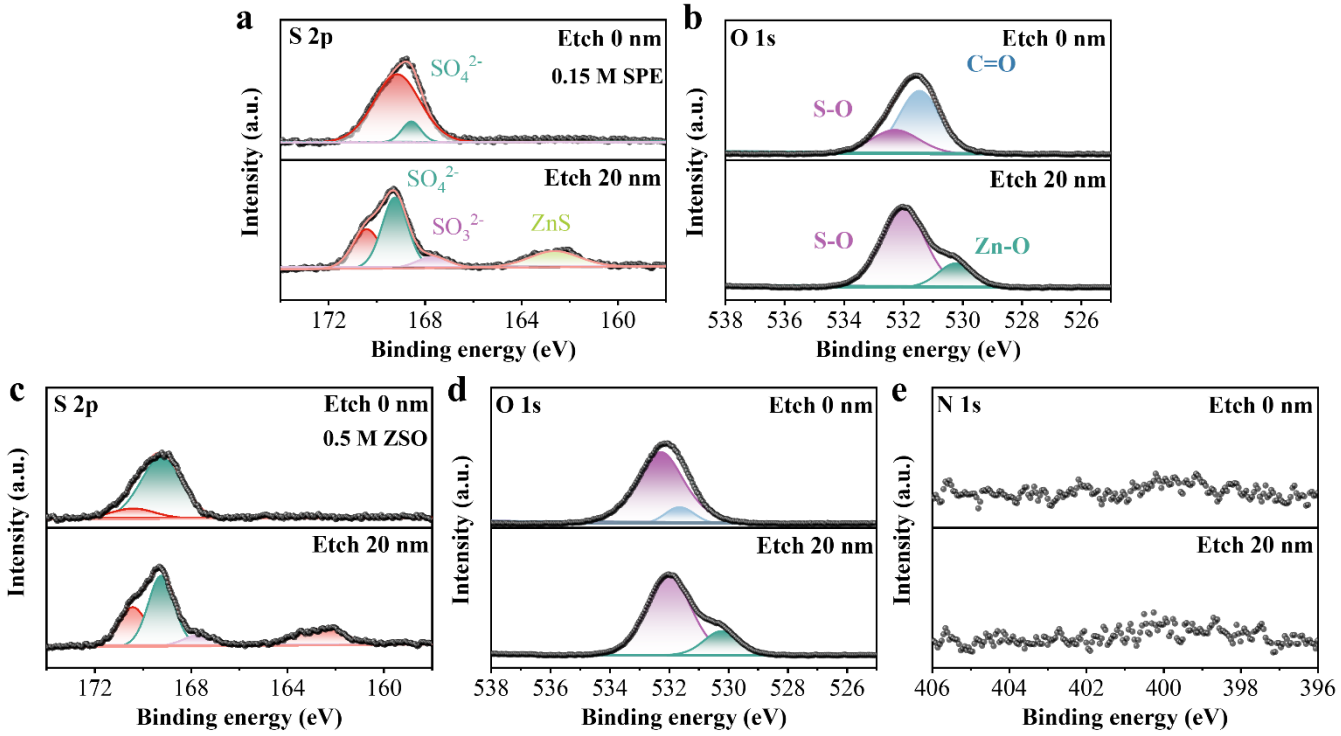

Figure S10 XPS a) S 2p spectra and b) O 1s spectra of deposited Zn anode collected from 0.15 M SPE, and XPS c) S 2p spectra, d) O 1s spectra and e) N 1s spectra of deposited Zn anode collected from 0.5 M ZSO.

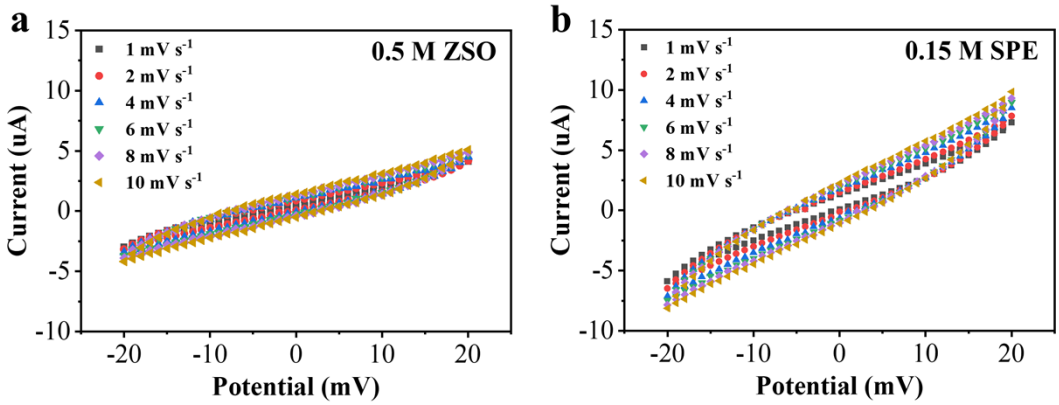

Figure S11. Electric double-layer capacitance measurement of Zn electrode. CV curves for Zn||Zn symmetric cell in the voltage range from −20 mV to 20 mV under various scanning rates in a) 0.5 M ZSO and b) 0.15 M SPE.

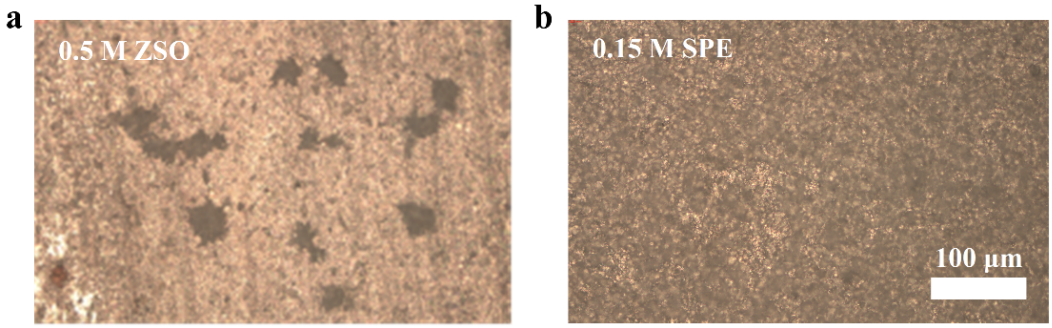

Figure S12. Optical microscopic images of Zn sheets after soaking in a) 0.5 M ZSO and b) 0.15 M SPE for 3 days.

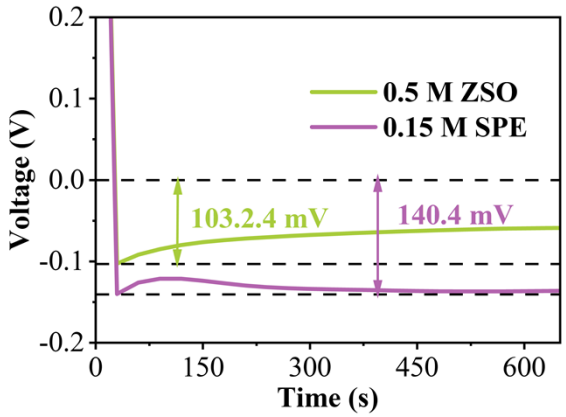

Figure S13. Capacity-voltage curves of Zn||Cu half-cell at initial cycle in 0.5 M ZSO and 0.15 M SPE.

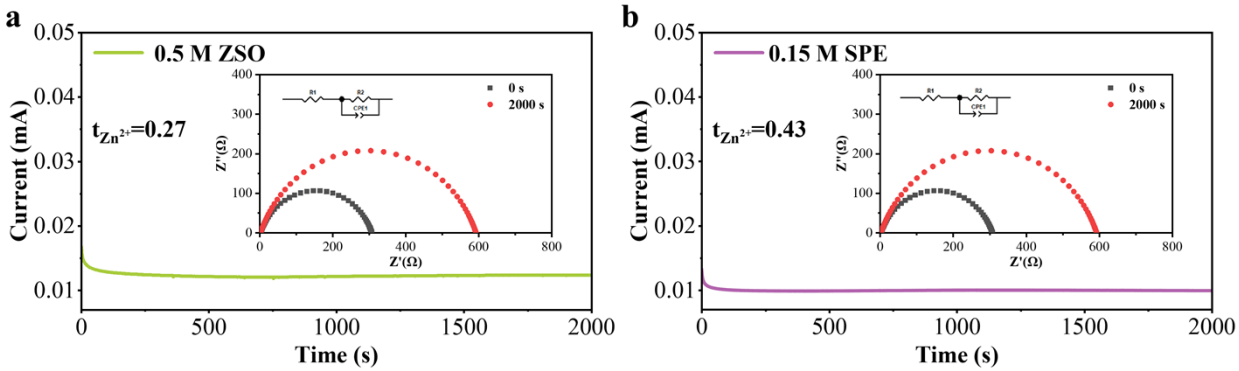

Figure S14. CA and EIS plots of Zn||Zn symmetric cells assembled with a) 0.5 M ZSO and b) 0.15 M SPE.

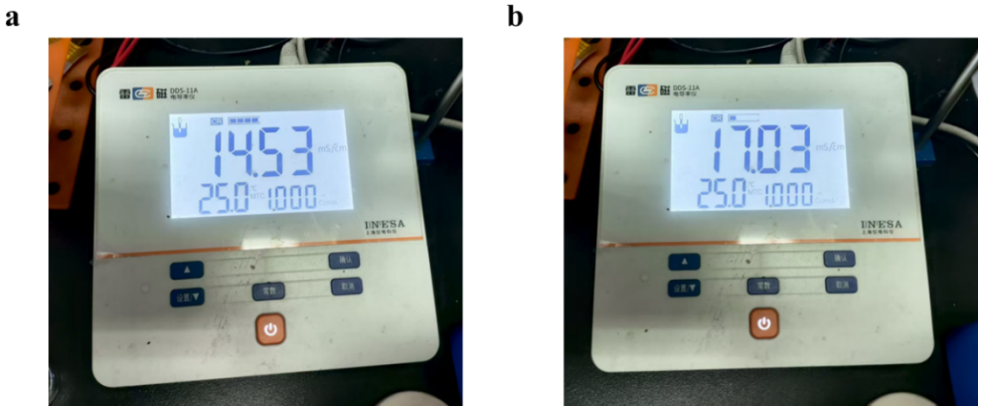

Figure S15. Photo of ionic conductivity test results of 0.5 M ZSO a) and 0.15 M SPE b) electrolytes.

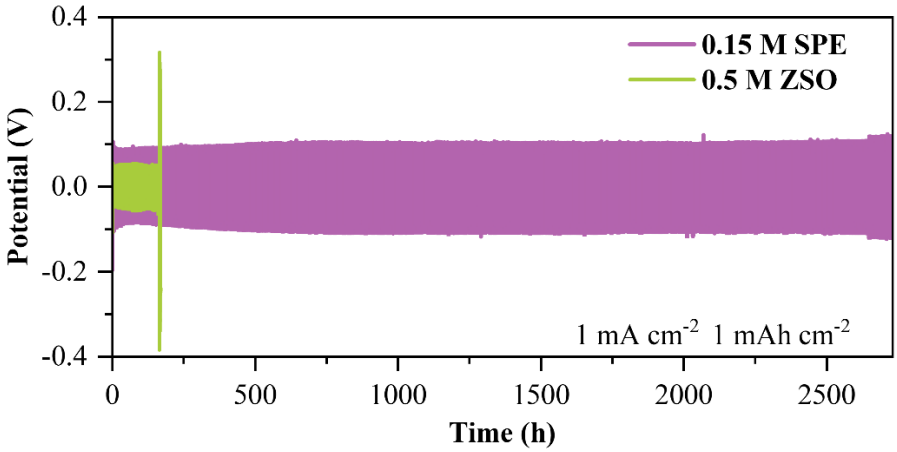

Figure S16. Cycle performance of Zn symmetric cells in electrolytes in 0.5 M ZSO and 0.15 M SPE electrolyte at 1 mA cm^{-2}, 1 mAh cm^{-2}.

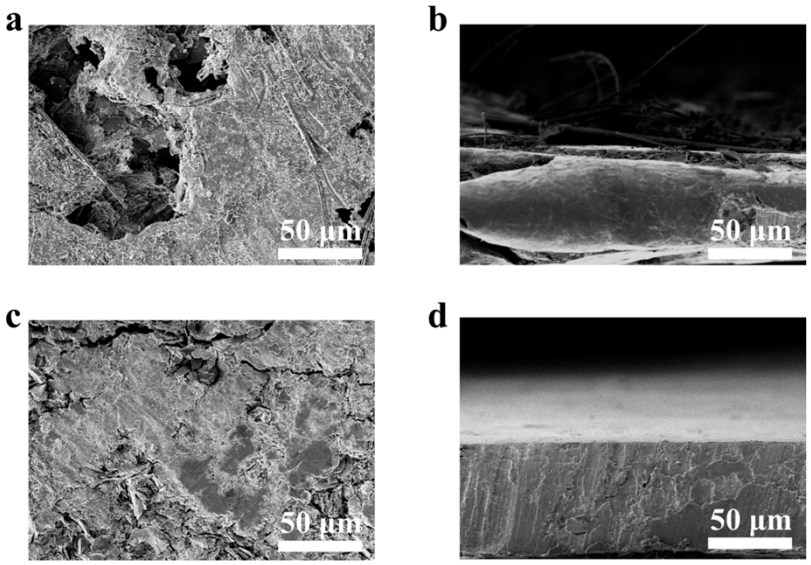

Figure S17. Planar and cross-sectional SEM images of Zn foils after cycling under high areal capacity (50 µm Zn foils, 25% DOD). a) Planar and b) cross-sectional images after cycling in 0.5 M ZSO, c) Planar and d) cross-sectional images after cycling in 0.15 M SPE.

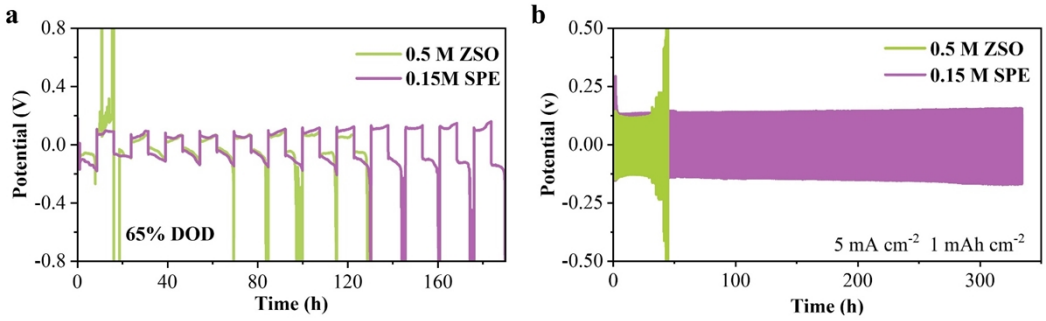

Figure S18. Cycling performance at high depth of discharge of Zn||Zn symmetric batteries using 20 µm Zn foil a) 65% DOD: 1 mA cm^{-2}, 7.61 mAh cm^{-2}, b) The battery cycling performance under high current density conditions. (5 mA cm^{-2}, 1 mAh cm^{-2})

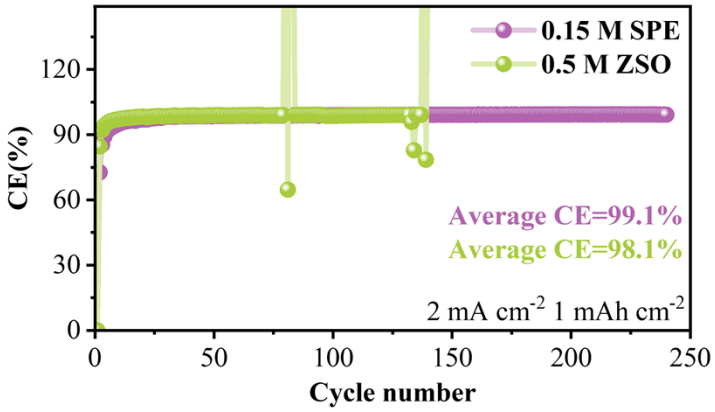

Figure S19. Cycling performance of Zn||Cu half-cells with 0.5 M ZSO and 0.15 M SPE electrolyte.

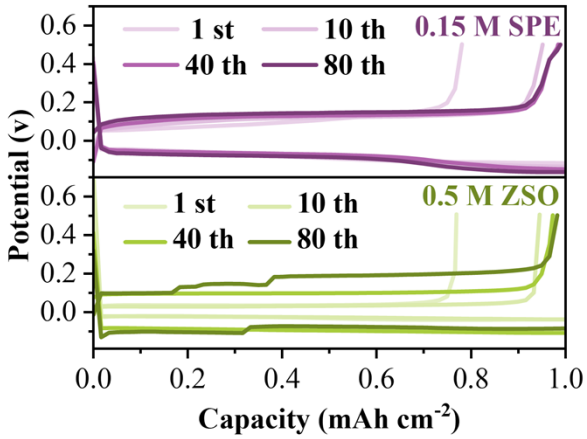

Figure S20. Voltage profiles of Zn||Cu cells in 0.5 M ZSO and 0.15 M SPE at 2 mA cm^{-2} and 1 mAh cm^{-2} at different cycles.

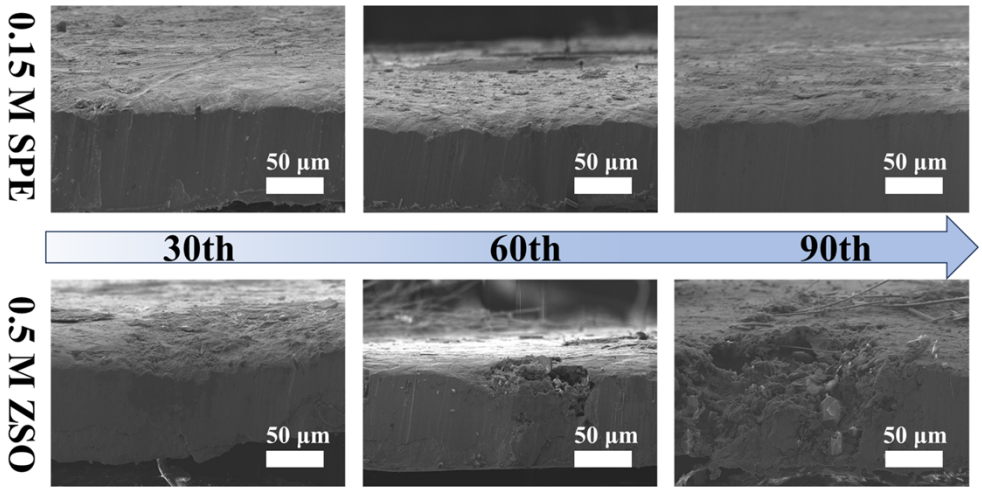

Figure S21. The cross-sectional SEM images a of the Zn foil surface after different cycles in 0.15 M SPE (top) and 0.5 M ZSO (bottom).

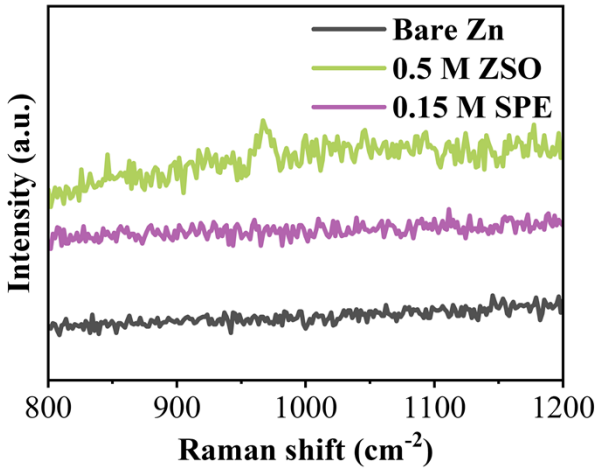

Figure S22. The Raman patterns of the Zn foil surface after 60 cycles in the 0.15 M SPE and 0.5 M ZSO.

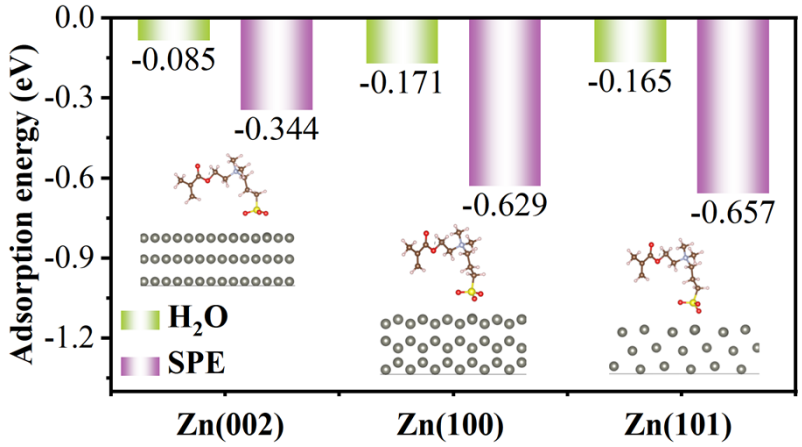

Figure S23. Absorption energy of SPE and H_2O molecules on Zn (002), (100) and (101) crystal planes.

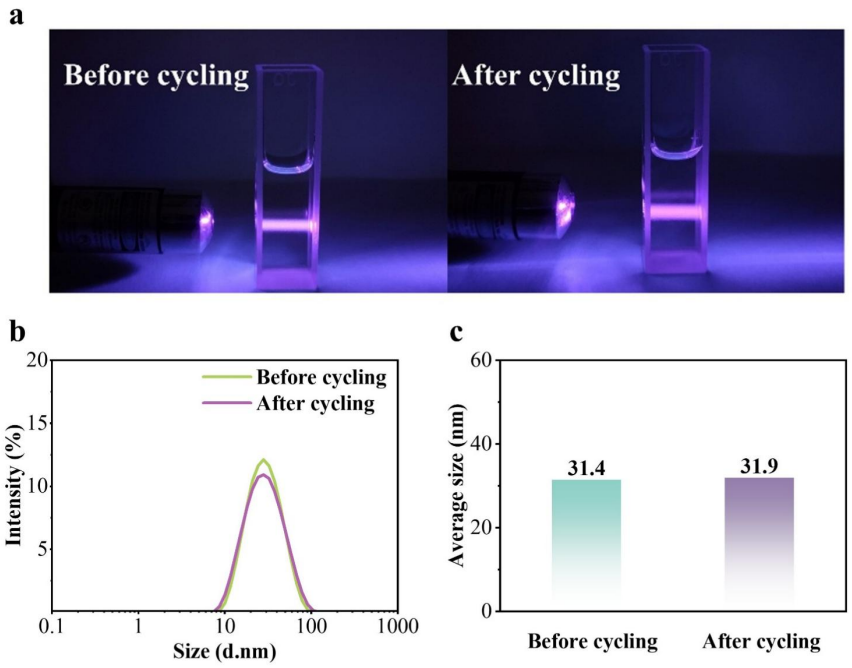

Figure S24. a) The Tyndall effect of the 0.15 M SPE electrolyte before and after circulation. b) DLS analysis of 0.15 M SPE electrolyte before and after cycling, and c) the corresponding average hydrodynamic size.

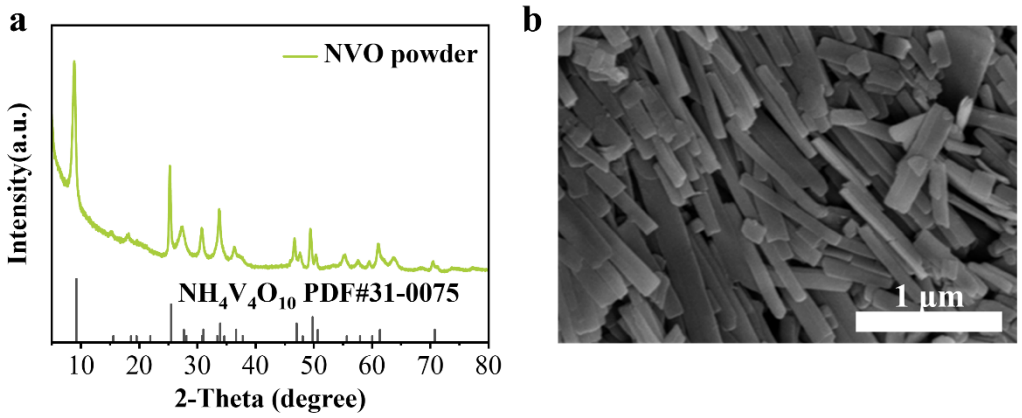

Figure S25. a) XRD patterns and b) SEM images of synthesized NVO powder.

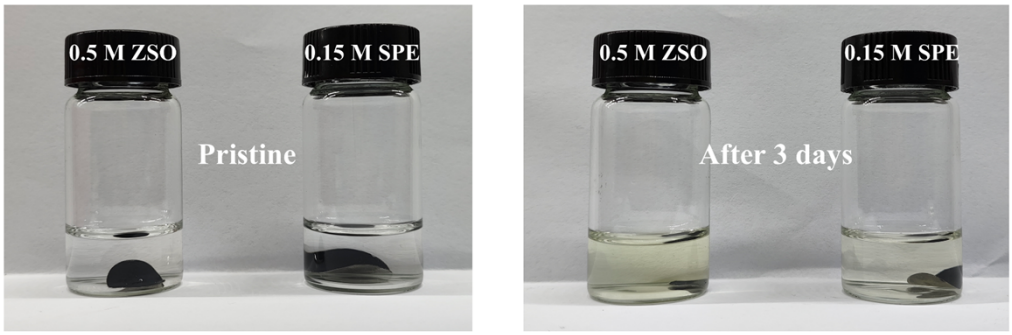

Figure S26. Optical images of electrolytes after soaking NVO electrodes for 3 days in 0.5 M ZSO and 0.15 M SPE electrolytes.

References

1. J. Chen, G. Ou, P. Liu, W. Fan, B. Li, Z. Hu, Z. Wen, Y. Zhang, Y. Tang, X. Liu, M. Ye and C. C. Li, *Angewandte Chemie International Edition*, 2025, **64**, e202414166.

2. T. Lu and F. Chen, *Journal of Computational Chemistry*, 2012, **33**, 580-592.

3. L. Martínez, R. Andrade, E. G. Birgin and J. M. Martínez, *Journal of Computational Chemistry*, 2009, **30**, 2157-2164.

4. F. Yssaad, F. Zineb, M. Dadouch, R. Aribi, F. Chater, K. Aicha and Y. Bouhadda, *Chemical Science Review and Letters*, 2025, **8**, 364-377.

5. Q. Gou, H. Luo, Q. Zhang, J. Deng, R. Zhao, O. Odunmbaku, L. Wang, L. Li, Y. Zheng, J. Li, D. Chao and M. Li, *Small*, 2023, **19**, 2207502.

6. Q. Deng, S. You, W. Min, Y. Xu, W. Lin, J. Lu and C. Yang, *Advanced Materials*, 2024, **36**, 2312924.